Sequence isomerism-dependent self-assembly of glycopeptide mimetics with switchable antibiofilm properties

Limin Chen,[ab] Jie Feng,[b] Dan Yang,[a] Falin Tian,[b] Xiaomin Ye,[b] Qiuping Qian,[b] Shuai Wei,*[c] and Yunlong Zhou*[ab]

[a] School of Ophthalmology and Optometry, Eye Hospital, School of Biomedical Engineering, Wenzhou Medical University, Wenzhou 325000, P. R. China

[b] Engineering Research Center of Clinical Functional Materials and Diagnosis & Treatment Devices of Zhejiang Province, Wenzhou Institute, University of Chinese Academy of Sciences, Wenzhou 325000, P. R. China

[c] Department of Chemistry, University of Michigan, Ann Arbor, Michigan 48109, United States

E-mail: *shuaiwei@umich.edu (S. W.) *zhouyl@wibe.ac.cn (Y. L. Z.)

Synthesis and characterization of glycopeptide mimetics

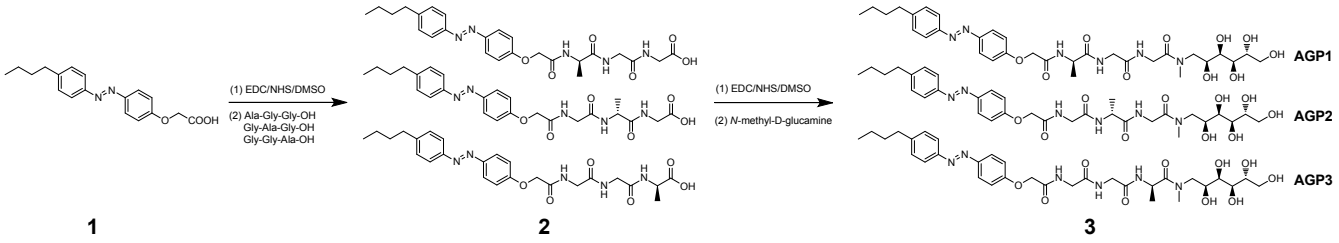

Scheme S1. Synthetic route of glycopeptide mimetics denoted as AGP1, AGP2 and AGP3.

1) Compound 1

Compound 1 was synthesized according to the reported protocols.[1]

2) Compound 2

N-(3-dimethylaminopropyl)-*N'*-ethylcarbodiimide hydrochloride (EDC) (614 mg, 3.2 mmol) and *N*-hydroxysuccinimide (NHS) (369 mg, 3.2 mmol) were added to 10 mL of DMSO containing compound 1 (1 g, 3.2 mmol). The mixture was incubated for 30 min before tripeptide (*i.e.,* Ala-Gly-Gly-OH, Gly-Ala-Gly-OH or Gly-Gly-Ala-OH) (650 mg, 3.2 mmol) was added. The reaction was allowed to proceed for 24 h at room temperature. Deionized water was added to the solution until a yellow precipitate formed. The compound 3 was purified by silica column chromatography using CH_3OH/CH_2Cl_2 (1/5, v/v) as eluent (~85% yield). ^{1}H NMR of *n*-butylazobenzene-Ala-Gly-Gly-OH (600 MHz, CD_3OD) δ (ppm): 7.91 (d, 2H, *J* = 12 Hz), 7.79 (d, 2H, *J* = 12 Hz), 7.34 (d, 2H, *J* = 12 Hz), 7.17 (d, 2H, *J* = 12 Hz), 4.69 (m, 2H), 4.48 (m, 1H), 3.90 (m, 4H), 2.70 (t, 2H), 1.66 (m, 2H), 1.45 (d, 3H), 1.40 (m, 2H), 0.96 (t, 3H). ^{1}H NMR of *n*-butylazobenzene-Gly-Ala-Gly-OH (600 MHz, CD_3OD) δ (ppm): 7.91 (d, 2H, *J* = 12 Hz), 7.79 (d, 2H, *J* = 12 Hz), 7.34 (d, 2H, *J* = 12 Hz), 7.17 (d, 2H, *J* = 12 Hz), 4.69 (s, 2H), 4.46 (m, 1H), 4.00 (s, 2H), 3.90 (m, 2H), 2.7 (t, 2H), 1.66 (m, 2H), 1.39 (m, 5H), 0.96 (t, 3H). ^{1}H NMR of *n*-butylazobenzene-Gly-Gly-Ala-OH (600 MHz,CD_3OD) δ (ppm): 7.91 (d, 2H, *J* = 12 Hz), 7.79 (d, 2H, *J* = 12 Hz), 7.34 (d, 2H, *J* = 12 Hz), 7.18 (d, 2H, *J* = 12 Hz), 4.70 (s, 2H), 4.40 (m, 1H), 4.01 (s, 2H), 3.93 (m, 2H), 2.70 (t, 2H), 1.66 (m, 2H), 1.40 (m, 5H), 0.96 (t, 3H).

3) Compound 3

EDC (384 mg, 2 mmol) and NHS (231 mg, 2 mmol) were added to 5 mL of DMSO containing compound 3 (1 g, 2 mmol). The mixture was incubated for 30 min before *N*-methyl-D-glucamine (390 mg, 2 mmol) was added. The reaction was allowed to proceed for 24 h at room temperature. Deionized water was added to the solution until a yellow gel-like agglomerates formed. The compound 3 was obtained by centrifugation and washed with water several times (~80% yield). ^{1}H NMR of AGP1 (600 MHz, CD_3OD) δ (ppm): 7.91 (d, 2H, *J* = 12 Hz), 7.79 (d, 2H, *J* = 12 Hz), 7.34 (d, 2H, *J* = 12 Hz), 7.17 (d, 2H, *J* = 12 Hz), 4.69 (m, 2H), 4.48 (m, 1H), 4.20 (m, 1H), 3.95 (m, 4H), 3.66 (m, 7H), 3.44 (m, 1H), 3.08 (s, 1H), 2.97 (s, 1H), 2.70 (t, 2H), 1.66 (m, 2H), 1.45 (d, 3H), 1.39 (m, 2H), 0.96 (t, 3H). ^{1}H NMR of AGP2 (600 MHz, CD_3OD) δ (ppm): 7.91 (d, 2H, *J* = 12 Hz), 7.79 (d, 2H, *J* = 12 Hz), 7.34 (d, 2H, *J* = 12 Hz), 7.18 (d, 2H, *J* = 12 Hz), 4.70 (s, 2H), 4.47 (m, 1H), 4.11 (m, 1H), 4.00 (m, 4H), 3.69 (m, 7H), 3.43 (m, 1H), 3.11 (s, 1H), 2.98 (s, 1H), 2.7 (t, 2H), 1.66 (m, 2H), 1.39 (m, 5H), 0.96 (t, 3H). ^{1}H NMR of AGP3 (600 MHz,CD_3OD) δ (ppm): 7.91 (d, 2H, *J* = 12 Hz), 7.79 (d, 2H, *J* = 12 Hz), 7.34 (d, 2H, *J* = 12 Hz), 7.18 (d, 2H, *J* = 12 Hz), 4.70 (d, 2H), 3.9 (m, 6H), 3.77 (m, 2H), 3.67 (m, 5H), 3.47 (m, 1H), 3.21 (s, 1H), 2.98 (s, 1H), 2.70 (t, 2H), 1.66 (m, 2H), 1.40 (m, 2H), 1.33 (m, 3H), 0.96 (t, 3H). The purity of compound 3 was analysed by reverse-phase HPLC on ZORBAX Eclipse Plus C18 Column (4.6 × 100 mm, 3.5 μm) using CH_3OH/H_2O (85/15, v/v) as eluent. Column flow = 1.00 mL min^{-1}.

4) Analytical reverse-phase HPLC of compound 3

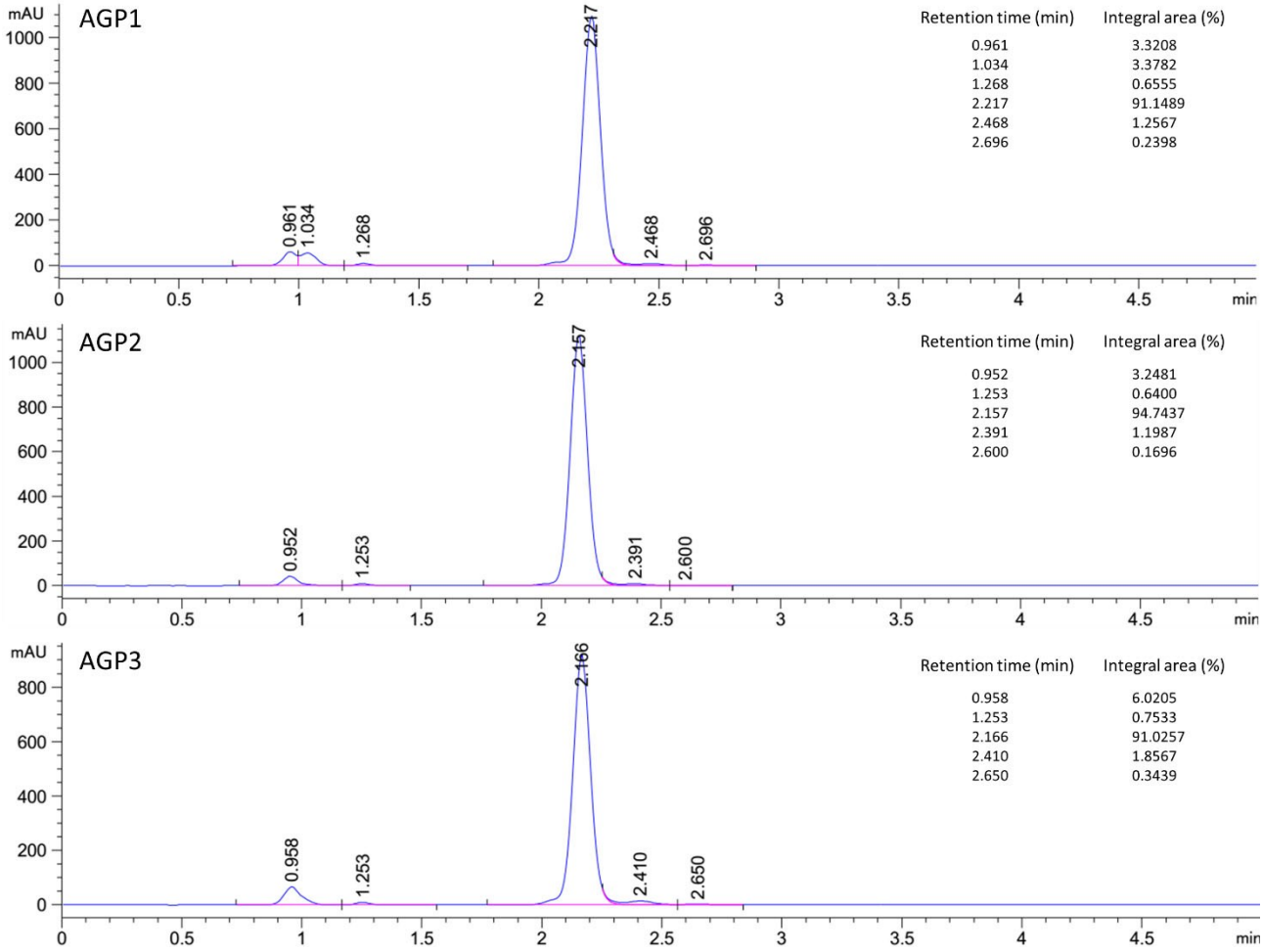

5) Electrospray ionization mass spectrometry of compound 3

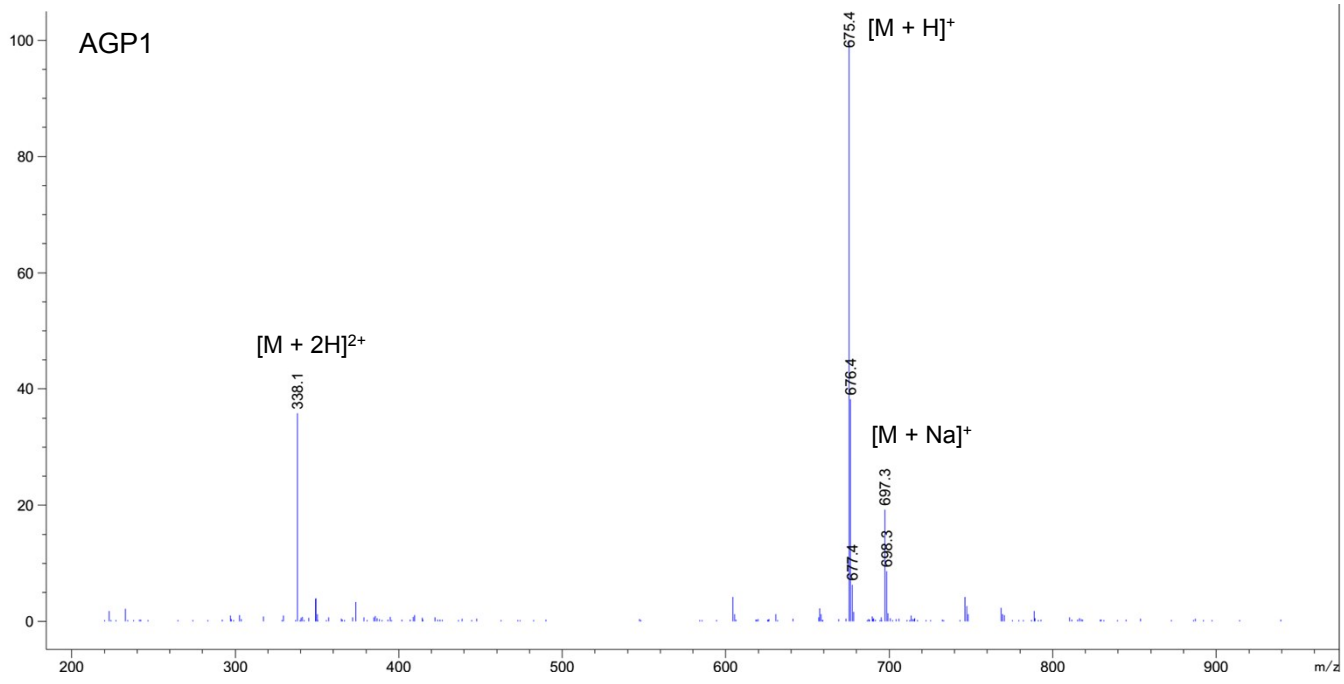

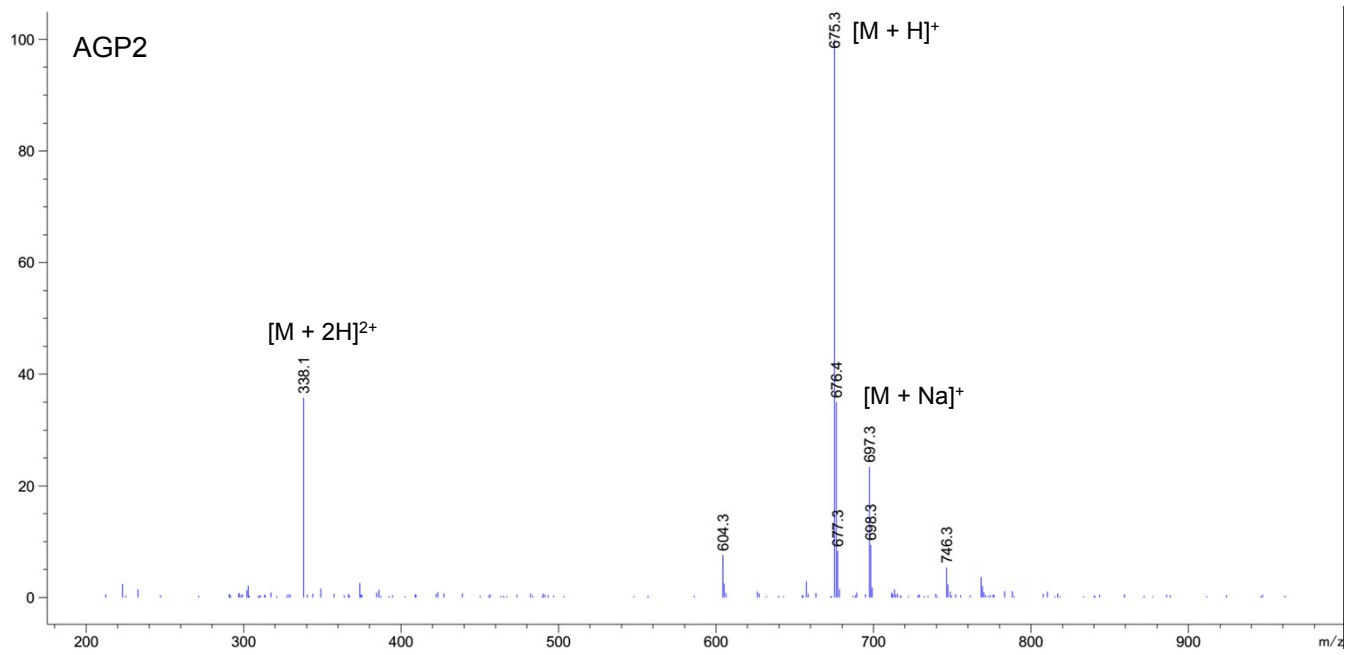
AGP2
[M + H]+
675.3
[M + 2H]2+
338.1
676.4
[M + Na]+
697.3
604.3
677.3
698.3
746.3
100
80
60
40
20
0
200
300
400
500
600
700
800
900
m/z

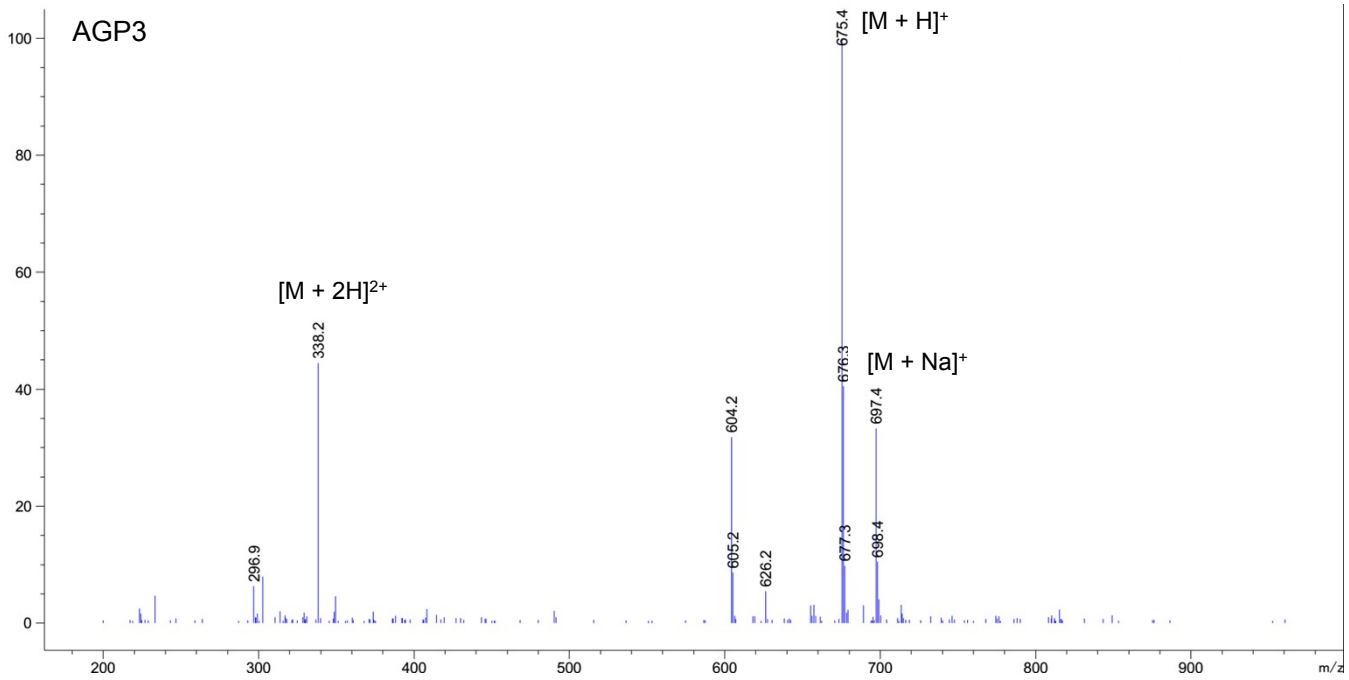
AGP3
[M + H]+
675.4
[M + 2H]2+
338.2
676.3
[M + Na]+
604.2
697.4
296.9
605.2
626.2
677.3
698.4
100
80
60
40
20
0
200
300
400
500
600
700
800
900
m/z

6) ^{1}H NMR spectra

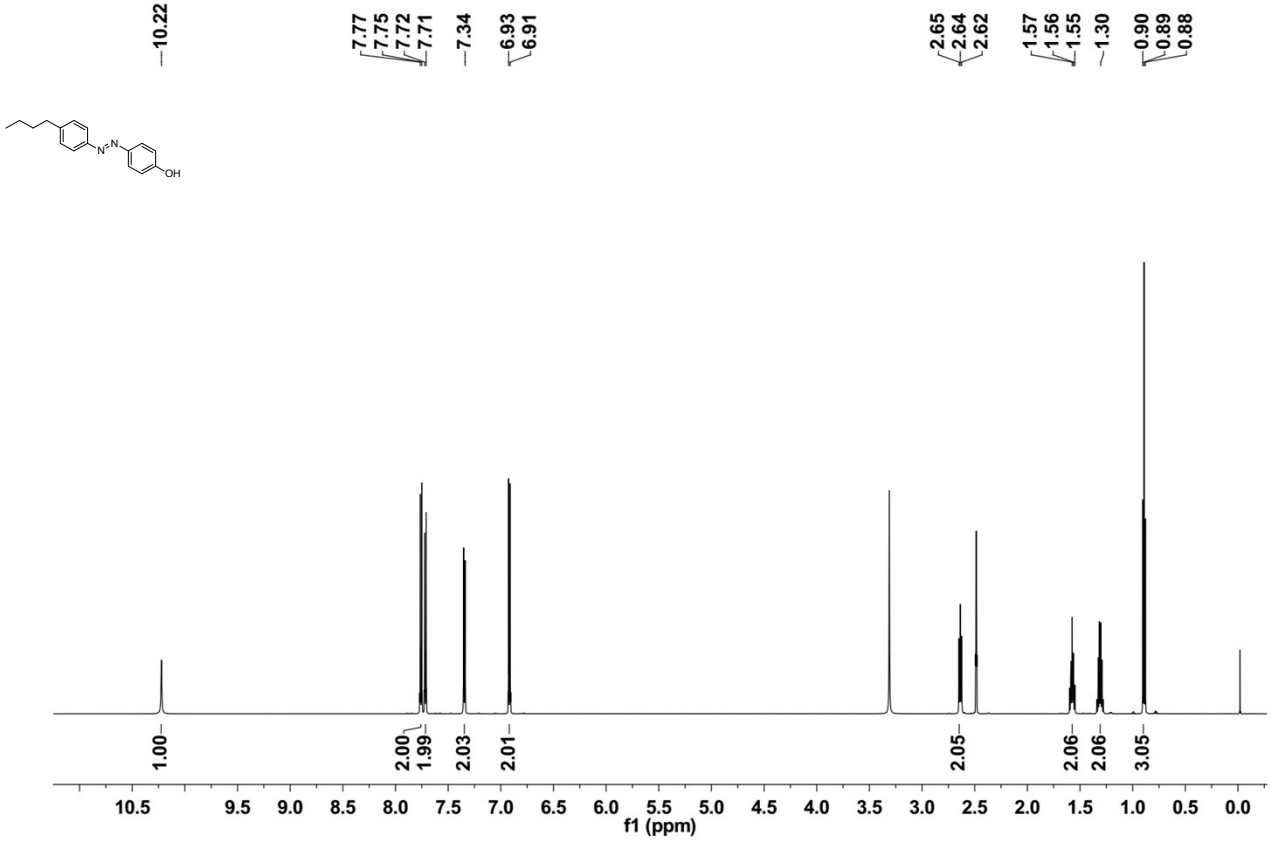

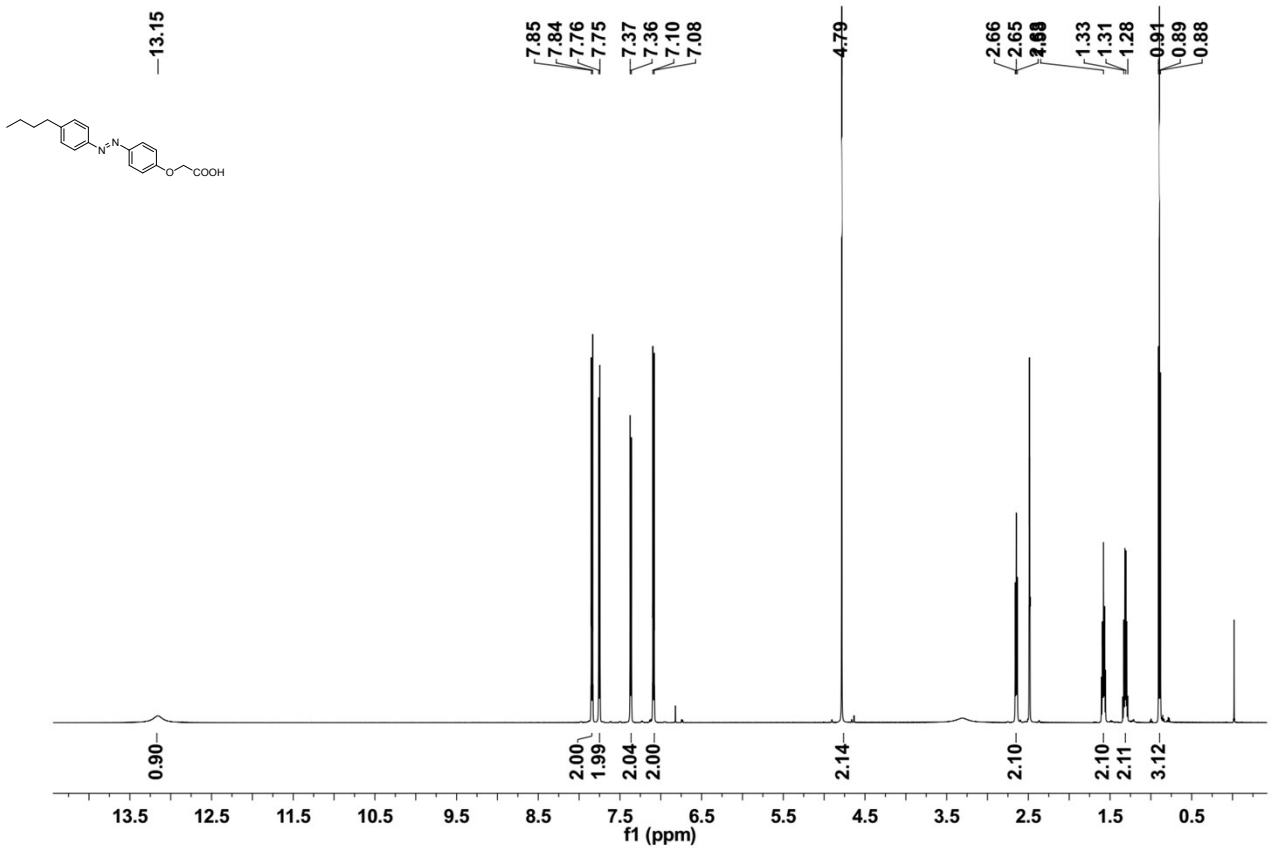

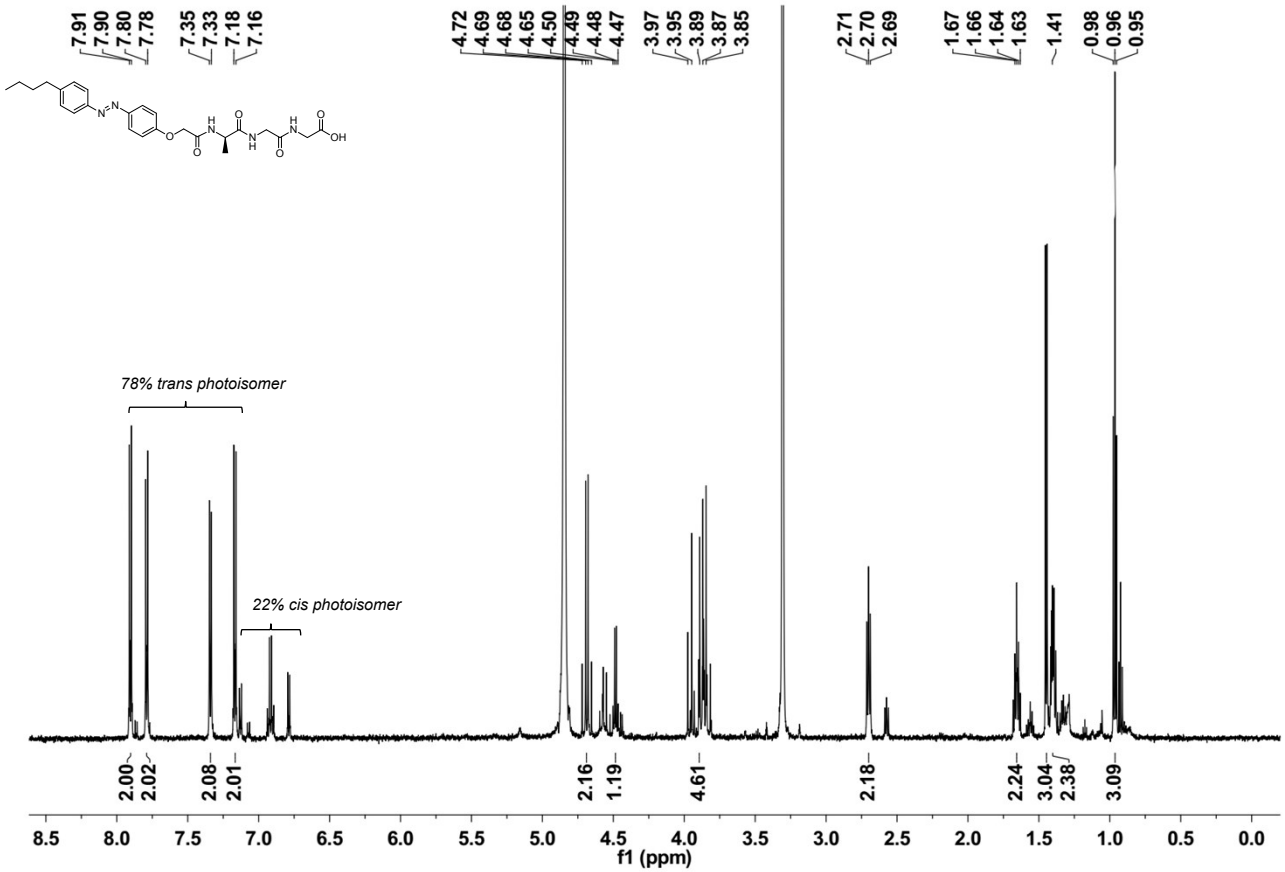
7.91
7.90
7.80
7.78
7.35
7.33
7.18
7.16
4.72
4.69
4.68
4.65
4.50
4.49
4.48
4.47
3.97
3.95
3.89
3.87
3.85
2.71
2.70
2.69
1.67
1.66
1.64
1.63
1.41
0.98
0.96
0.95
78% trans photoisomer
22% cis photoisomer
2.00
2.02
2.08
2.01
2.16
1.19
4.61
2.18
2.24
3.04
2.38
3.09
8.5
8.0
7.5
7.0
6.5
6.0
5.5
5.0
4.5
4.0
3.5
3.0
2.5
2.0
1.5
1.0
0.5
0.0
f1 (ppm)

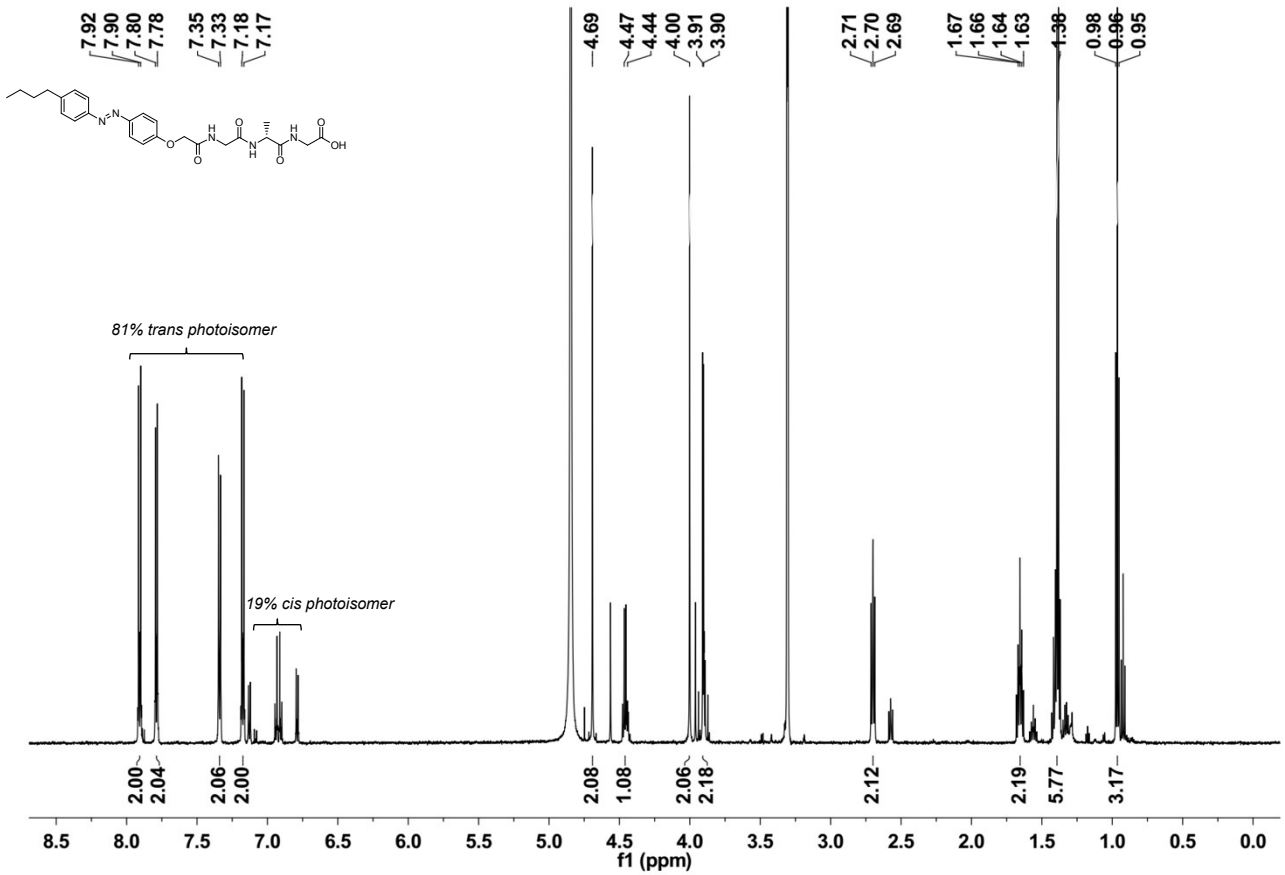
7.92
7.90
7.80
7.78
7.35
7.33
7.18
7.17
4.69
4.47
4.44
4.00
3.91
3.90
2.71
2.70
2.69
1.67
1.66
1.64
1.63
1.38
0.98
0.96
0.95
81% trans photoisomer
19% cis photoisomer
2.00
2.04
2.06
2.00
2.08
1.08
2.06
2.18
2.12
2.19
5.77
3.17
8.5
8.0
7.5
7.0
6.5
6.0
5.5
5.0
4.5
4.0
3.5
3.0
2.5
2.0
1.5
1.0
0.5
0.0
f1 (ppm)

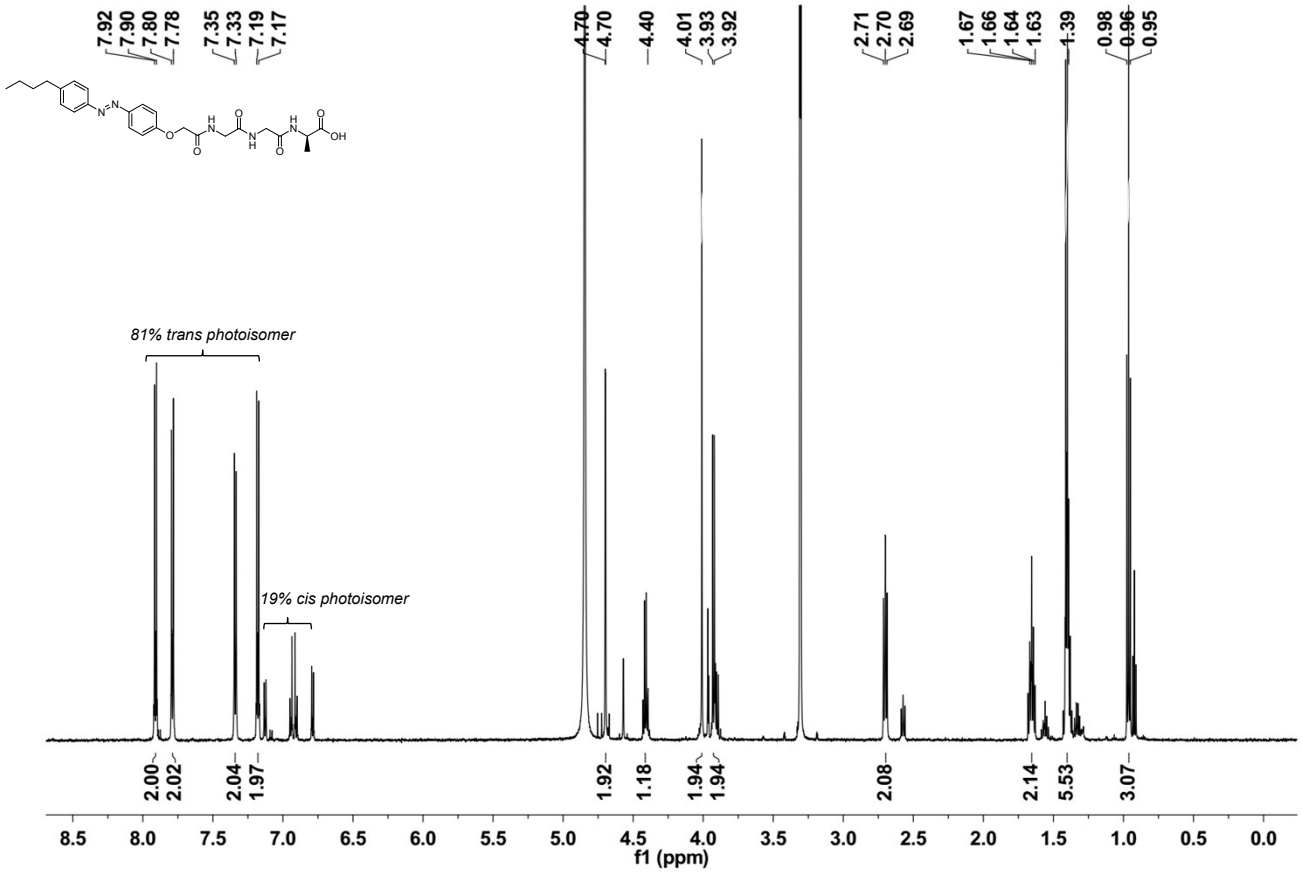
7.92
7.90
7.80
7.78
7.35
7.33
7.19
7.17
4.70
4.70
4.40
4.01
3.93
3.92
2.71
2.70
2.69
1.67
1.66
1.64
1.63
1.39
0.98
0.96
0.95
81% trans photoisomer
19% cis photoisomer
2.00
2.02
2.04
1.97
1.92
1.18
1.94
1.94
2.08
2.14
5.53
3.07
8.5
8.0
7.5
7.0
6.5
6.0
5.5
5.0
4.5
4.0
3.5
3.0
2.5
2.0
1.5
1.0
0.5
0.0
f1 (ppm)

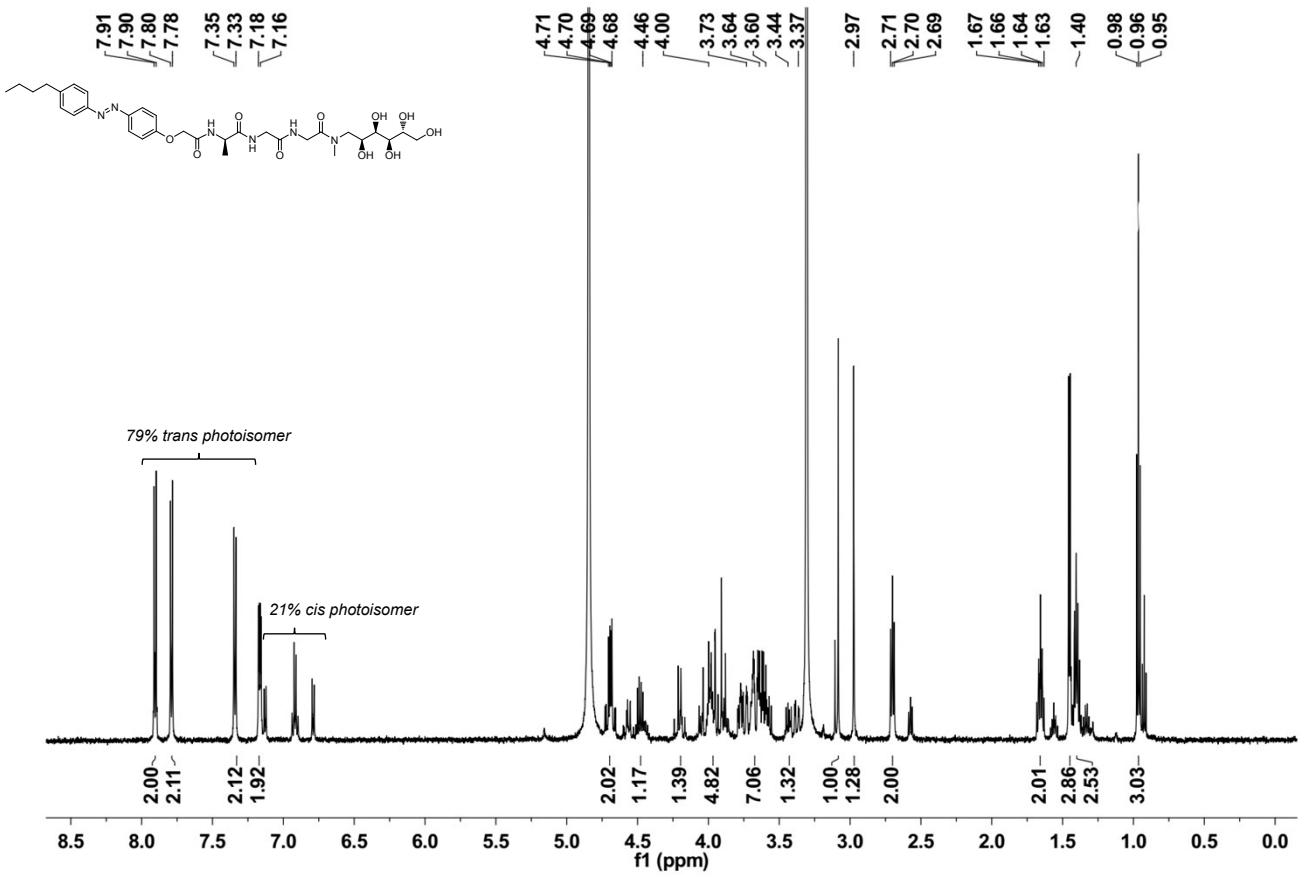
7.91
7.90
7.80
7.78
7.35
7.33
7.18
7.16
4.71
4.70
4.69
4.68
4.46
4.00
3.73
3.64
3.60
3.44
3.37
2.97
2.71
2.70
2.69
1.67
1.66
1.64
1.63
1.40
0.98
0.96
0.95
79% trans photoisomer
21% cis photoisomer
2.00
2.11
2.12
1.92
2.02
1.17
1.39
4.82
7.06
1.32
1.00
1.28
2.00
2.01
2.86
2.53
3.03
8.5
8.0
7.5
7.0
6.5
6.0
5.5
5.0
4.5
4.0
3.5
3.0
2.5
2.0
1.5
1.0
0.5
0.0
f1 (ppm)

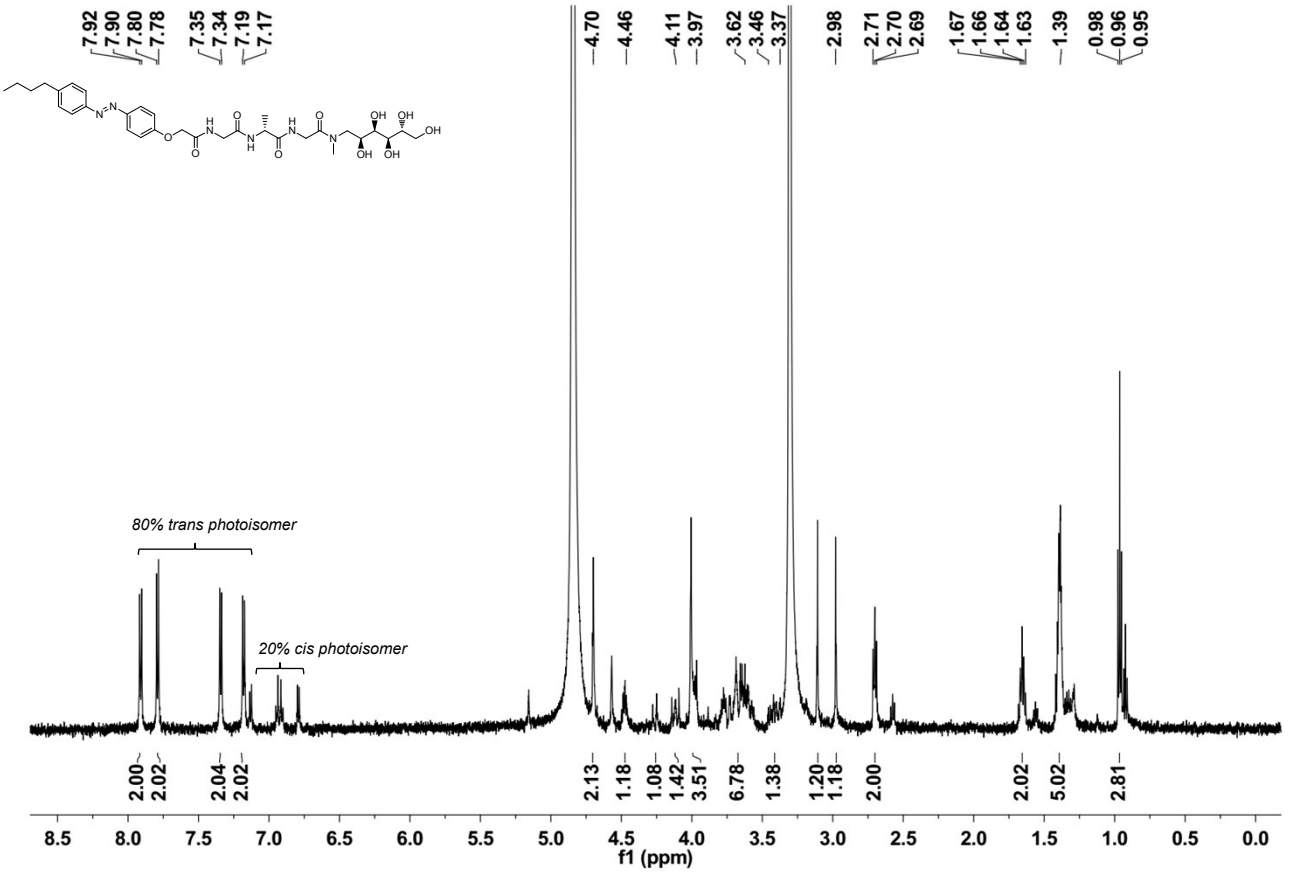
7.92
7.90
7.80
7.78
7.35
7.34
7.19
7.17
4.70
4.46
4.11
3.97
3.62
3.46
3.37
2.98
2.71
2.70
2.69
1.67
1.66
1.64
1.63
1.39
0.98
0.96
0.95
80% trans photoisomer
20% cis photoisomer
2.00
2.02
2.04
2.02
2.13
1.18
1.08
1.42
3.51
6.78
1.38
1.20
1.18
2.00
2.02
5.02
2.81
f1 (ppm)

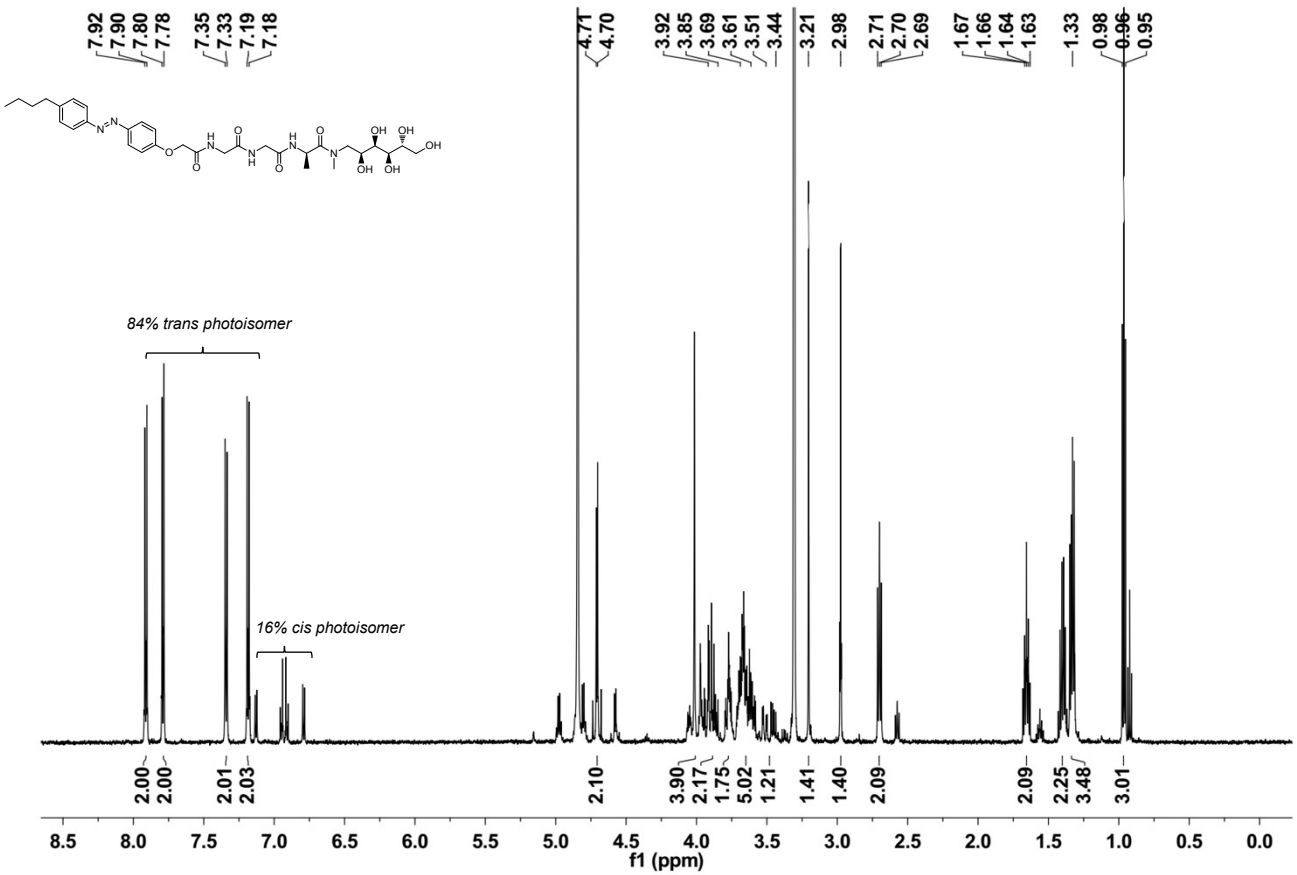
7.92
7.90
7.80
7.78
7.35
7.33
7.19
7.18
4.71
4.70
3.92
3.85
3.69
3.61
3.51
3.44
3.21
2.98
2.71
2.70
2.69
1.67
1.66
1.64
1.63
1.33
0.98
0.96
0.95
84% trans photoisomer
16% cis photoisomer
2.00
2.00
2.01
2.03
2.10
3.90
2.17
1.75
5.02
1.21
1.41
1.40
2.09
2.09
2.25
3.48
3.01
f1 (ppm)

Experimental methods

1) To prepare solution samples, the AGP powders were fully dissolved in water at desired concentrations at 70 °C before being cooled to room temperature for self-assembly. 3 mM of AGP molecules in water starts to form a hydrogel according to the inversion tests.

2) TEM samples were prepared as follows: 5 μL of solution sample (0.6 mM) was deposited onto a carbon-coated copper grid. The excess of the solution was quickly wicked away by a piece of filter paper, and the sample was subsequently left to dry in air. Once dried, the sample was negatively stained by placing a drop of 2wt% uranyl acetate aqueous solution on the top, and the excess was quickly blotted away to leave a thin layer of uranyl acetate solution. Again, the sample was left to dry under ambient conditions. TEM imaging of self-assembled nanostructures was performed on JEOL 2100F at an accelerating voltage of 200 kV. The average width (indicating stdev) of nanostructures was obtained by measuring ~100 structures in TEM images using a Nano Measurer 1.2 software.

3) For preparation of AFM samples, 20 μL of solution sample (0.6 mM) was deposited onto a silica plate (1 cm × 1 cm) for 3 min. The excess of the solution was absorbed away by a piece of filter paper, and the sample was subsequently left to dry. AFM imaging of self-assembled nanostructures was performed on a Bruker Dimension Icon instrument in contact mode in air. The height profiles in the AFM images were measured using a Bruker NanoScope Analysis software. The average height (indicating stdev) of nanostructures was obtained by measuring ~100 structures in AFM images.

4) Rheological experiments were performed on AGP hydrogels (30 mM) at 25 °C with a rheometer (DHR-2, TA instruments) using steel parallel-plate geometry (25 mm diameter). Strain sweep at a constant angular frequency (1 rad/s) was performed in the 0.1-100% range. Frequency sweep was obtained from 0.1 to 10 rad/s at a constant strain of 1%. Gel kinetics was obtained by measuring the *G'* and *G''* as a function of cooling time with a constant strain value of 1% and angular frequency of 1 rad/s.

5) XRD samples were obtained by drying hydrogels (30 mM) in air at room temperature. XRD analysis of air-dried samples was performed on a Bruker D8 Advance X-ray diffractometer with $Cu_{K\alpha}$ radiation (λ = 1.5418Å), which was operated at a voltage of 40 kV and a current of 40 mA.

6) For preparation of FT-IR samples, AGP hydrogels (30 mM) were prepared by fully dissolving the powders in D_2O at 70 °C before being cooled at room temperature for self-assembly. AGP/β-CyD samples were prepared by adding β-CyD ($n_{\beta\text{-CyD}} : n_{\mathbf{AGP}} = 8 : 1$) to AGP assemblies (0.6 mM) and dried in air at room temperature. FT-IR spectra were acquired on a Bruker Tensor II FT-IR spectrometer in attenuated total reflection (ATR) mode, with the wavenumber scanned between 4000 and 400 cm^{-1}, and a wavenumber resolution of 4 cm^{-1}.

7) CD/UV spectra of solution samples (0.6 mM) upon response to heat, light or host-guest chemistry were acquired on Applied Photophysics Chirascan Plus spectrophotometer. In multiple cycle experiments, CD signals of azobenzene were monitored at a specific wavelength (AGP1: 331 nm; AGP2: 374 nm; AGP3: 352 nm) upon response to temperature changes or alternating UV/Vis illumination. The reversible process was repeated 3 cycles.

8) To determine the critical aggregation concentration (CAC) values of AGP molecules, CD spectra of AGP self-assembly solutions at gradually increasing concentrations were recorded (Fig. S6). We plotted the CD signals of azobenzene (AGP1: 331 nm; AGP2: 374 nm; AGP3: 352 nm) as a function of concentration values (Fig. S6). The CAC values were obtained from the intersection of lines extrapolated from CD signal values in the near pre- and post-CAC regions (Fig. S6). It is rational to use CD spectroscopy to determine CAC values of AGP molecules, based on the following principle: The non-assembling AGP molecules in solution state did not give any CD signal of azobenzene due to the free state of azobenzene in solution, while the AGP assemblies showed CD signals of azobenzene due to transfer of chiral information from chiral center (Ala) to chromophore (azobenzene) originated from the self-assembly of AGP molecules.

Rheological properties of AGP hydrogels

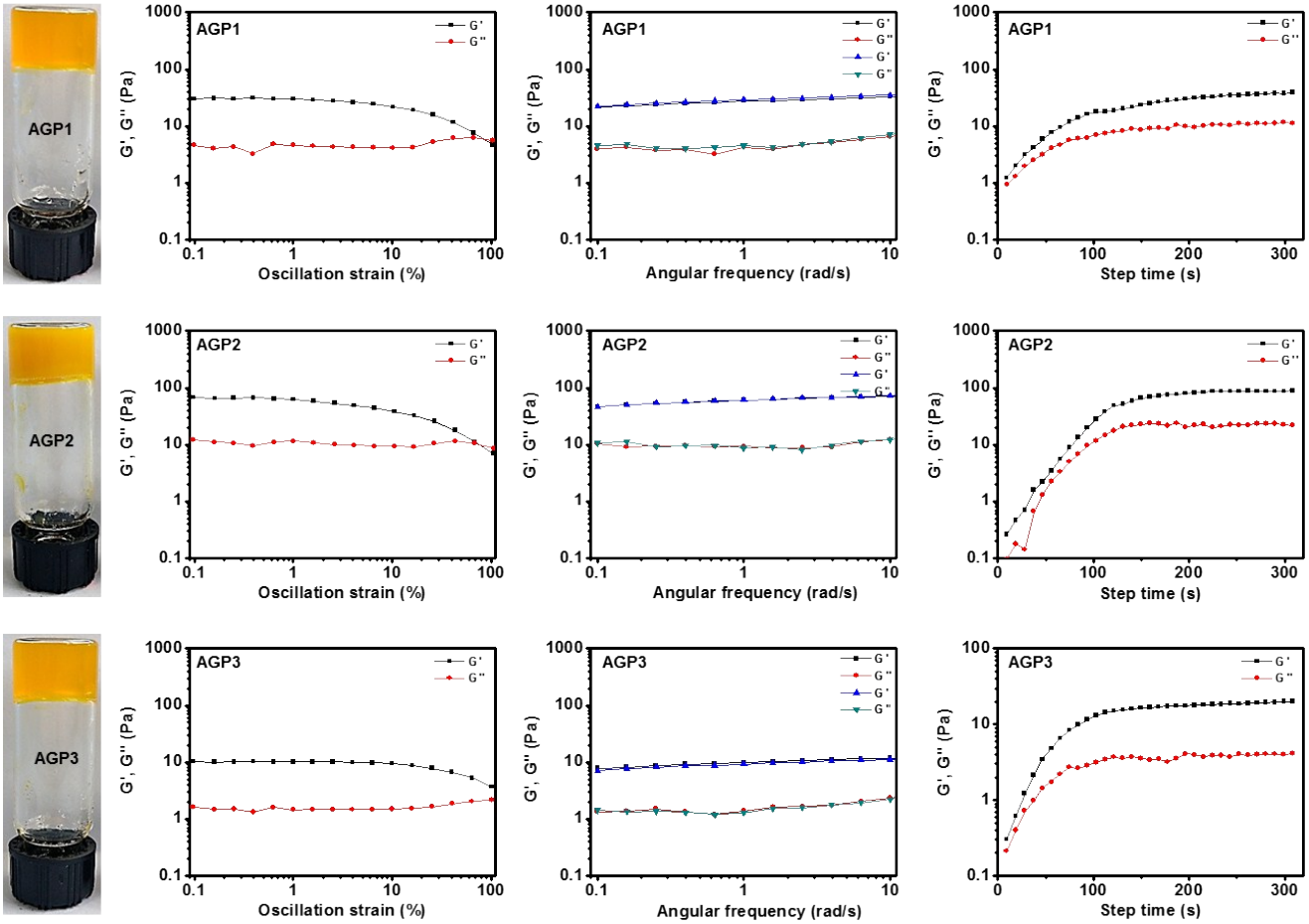

Fig. S1 Rheological properties of AGP hydrogels (30 mM).

Nanostructure dimensions

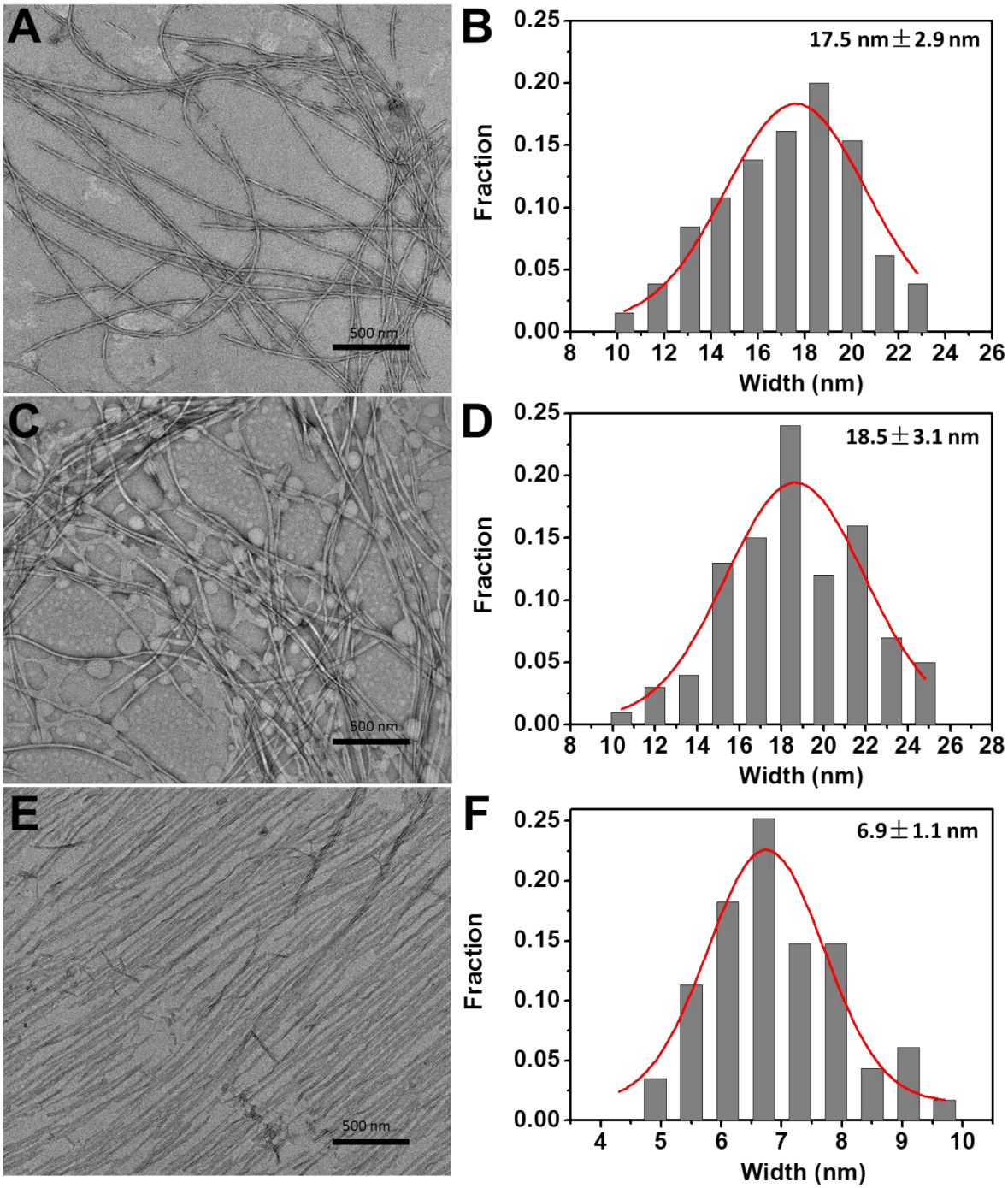

Fig. S2 Representative TEM images and the average width of AGP1 (A, B), AGP2 (C, D), AGP3 (E, F) assemblies.

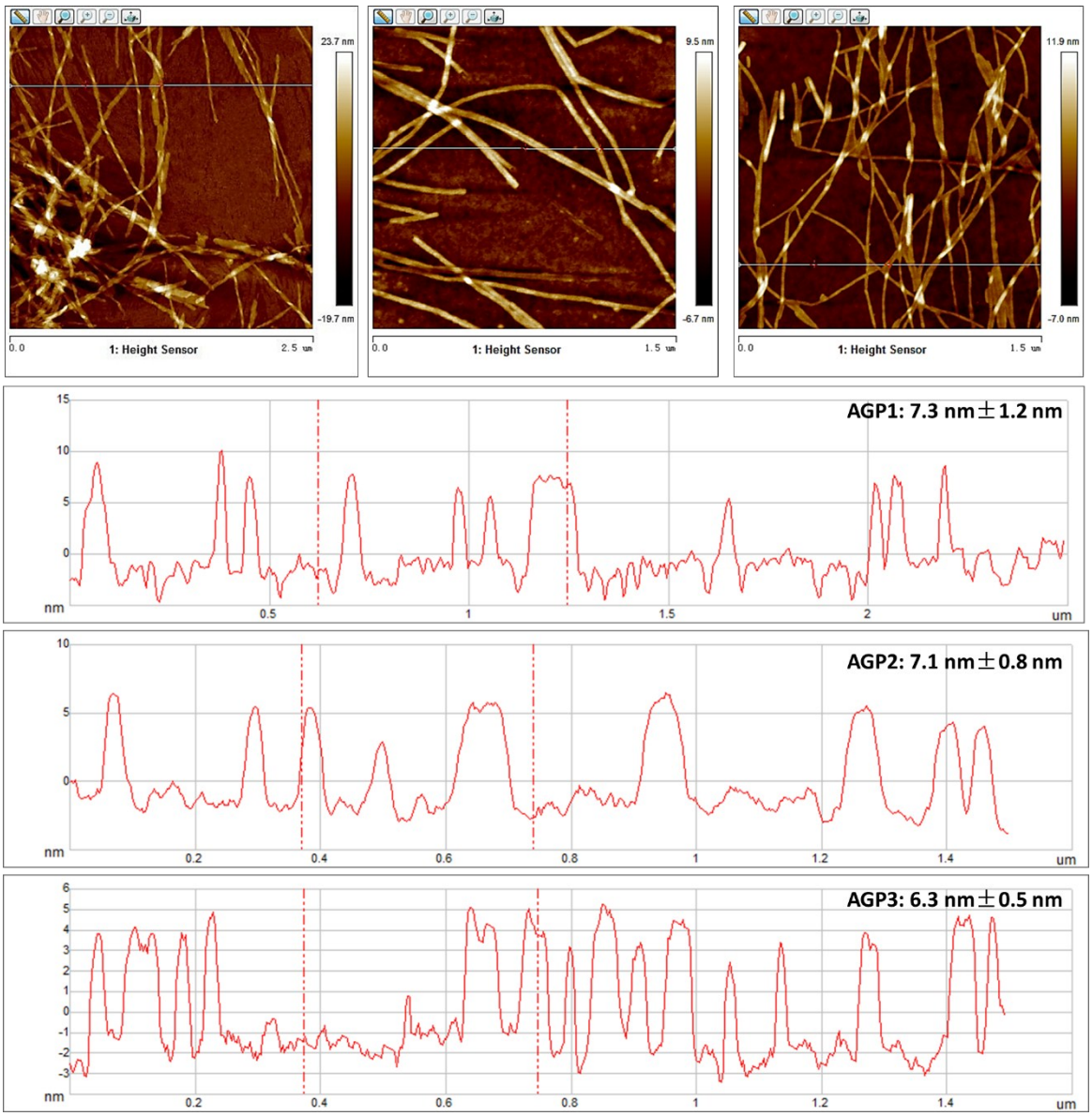

Fig. S3 Representative height profiles along the lines in the AFM images and the average height of AGP assemblies.

CPK molecular model

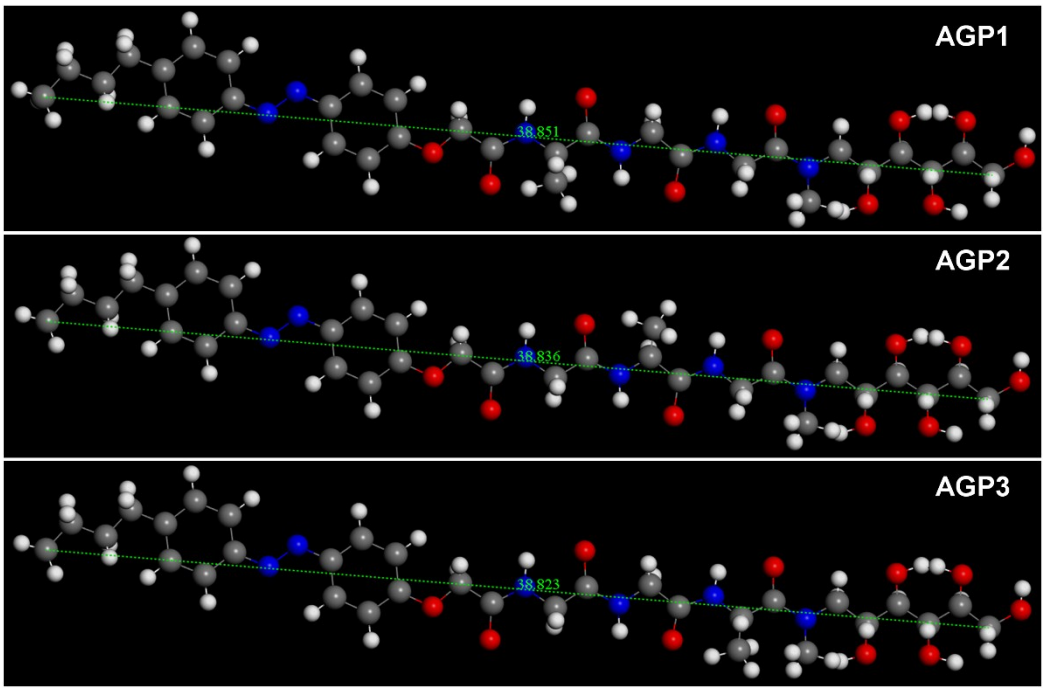

Fig. S4 The extended molecular length of AGP molecules estimated by CPK molecular model using Materials Studio 8.0 software.

FT-IR spectra

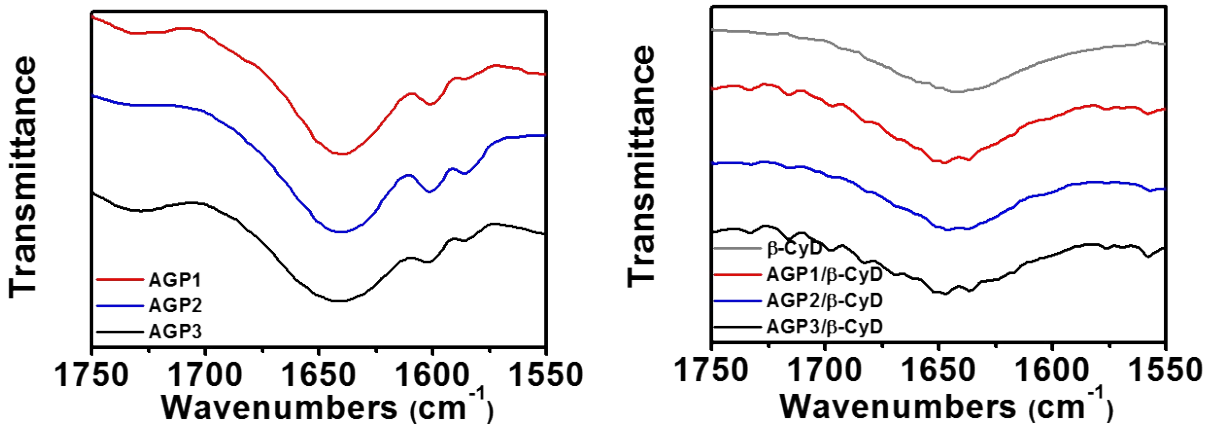

Fig. S5 FT-IR spectra of AGP hydrogels in D_2O or air-dried AGP/β-CyD samples.

Critical aggregation concentration (CAC)

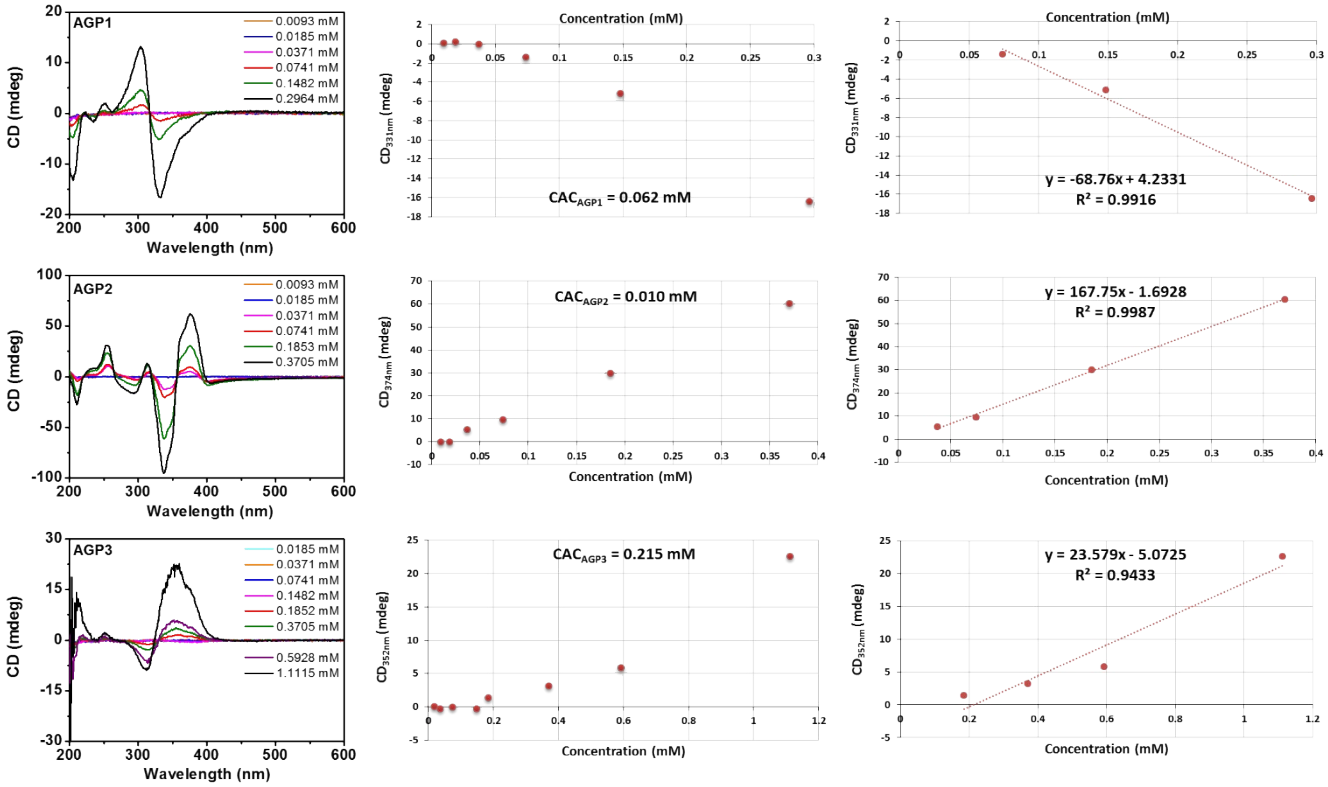

Fig. S6 CD spectroscopy characterization of the CAC values of AGP molecules in water.

Reversible disassembly-assembly properties of AGP assemblies

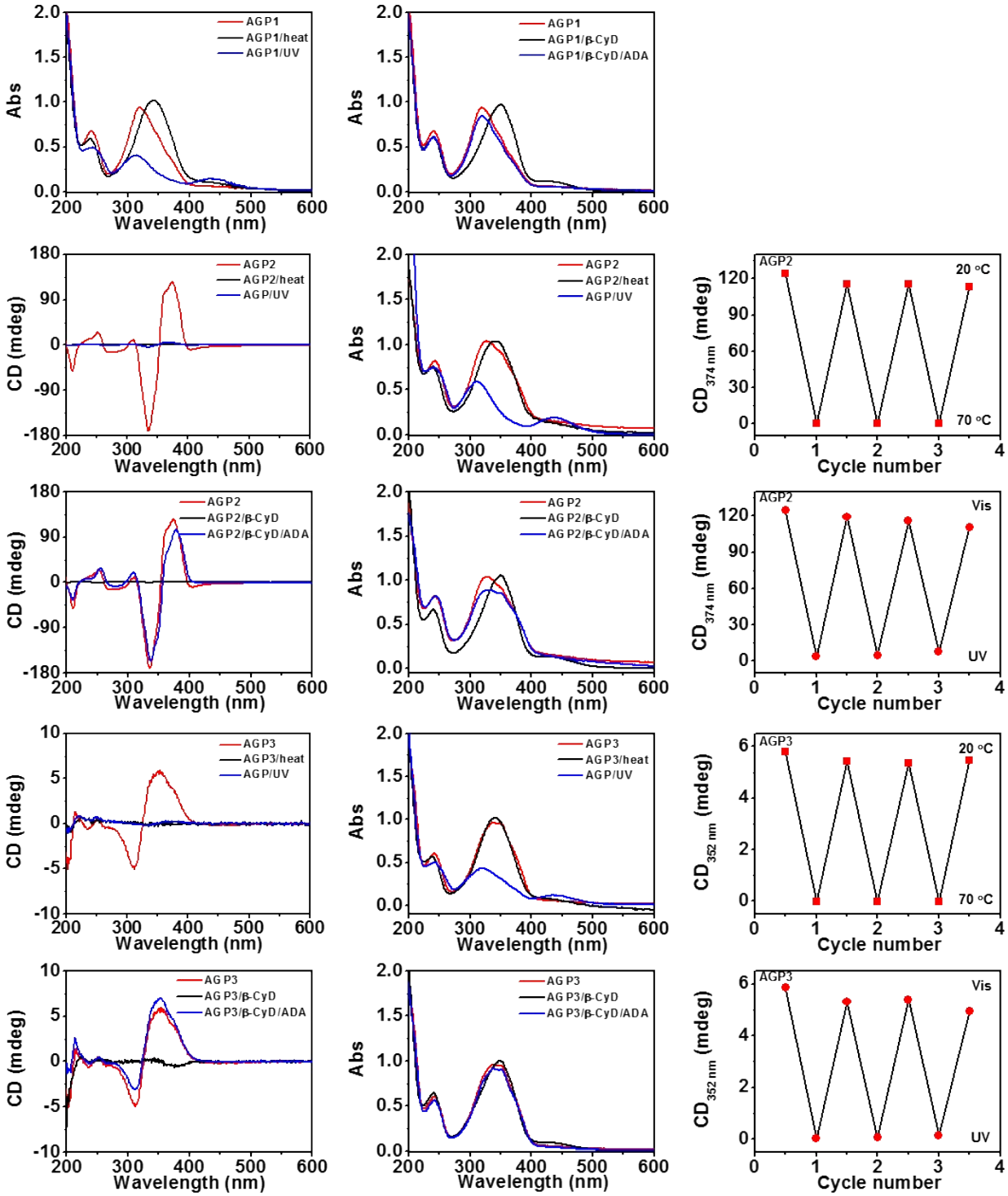

Fig. S7 CD/UV-Vis spectroscopy characterization of AGP assemblies (0.6 mM) upon response to temperature, light or host-guest chemistry.

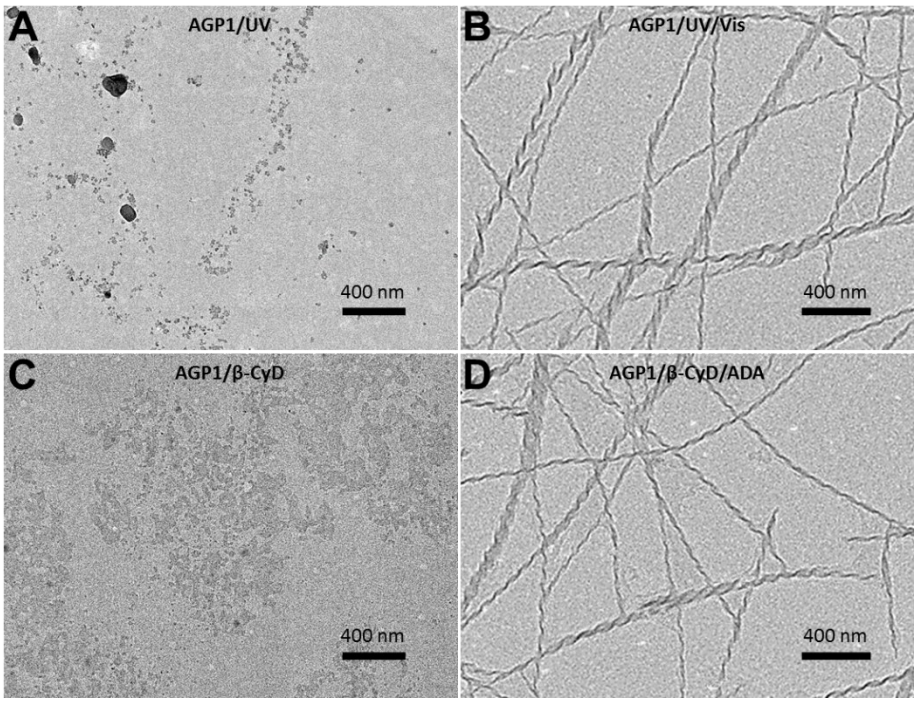

Fig. S8 TEM imaging of AGP1 assemblies upon alternating UV/Vis photoirradiation (A, B), or host-guest interactions (C, D).

Molecular dynamics (MD) simulations

1) Atomistic simulation and Coarse-graining of bi-molecule systems

The molecular structures and initial conformations were constructed and energy-minimized by using Avogadro software.[2] The resulting pdb structural files were then fed into the VMD force field toolkit.[3] The resulting parameter and structural files were used for atomistic simulations using the computational software Gromacs.[4]

The goal of performing atomistic MD simulation is to sample the intra- and inter-actions between a pair of molecules in each case. With the trajectory of the sufficiently sampled interactions between each pair of molecules, we could build the coarse-grained models for large-scale self-assembly simulations. However, direct MD simulations were not time-efficient for that goal. To enhance such samplings, we used Metadynamics sampling method[5] with the PLUMED2[6] software through Gromacs.

Followed by the atomistic simulations, we used the PyCGTOOL to automatically construct the Martini CG models via calculating both interactive equilibrium and force constants of internal coordinates from the Metadynamics atomistic MD simulation trajectory.[7] The mappings from atoms to Martini coarse-grained typed beads are based on the general rules for macromolecules and proteins as listed in Fig. S9.[8] Parameters were obtained based on the interactive bi-molecule systems atomistic simulations as shown in Fig. S10A resulting in the representative conformation in Fig. S10B.[9] To understand the potential allosteric effect from the Ala side-chain (compared to two Gly residues), an extra small bead was used for the side-chain. In this work, we only modeled L-Ala in the coarse-grained simulation to study effects of the residue relative positions on fiber morphologies.

2) Coarse-grained simulation of molecule self-assembly with different system sizes

As discussed in the main text, simulations with small number of molecules were performed for all three types. Fig. S10C demonstrated the formation of the di-molecule layer by AGP1 with 32 molecules. It represented the generic formation for all three types of molecules. Again, the medium sized simulation system with 192 molecules formed this "Y"-shape structure, which is identical to the structure found at the interfaces of subunit cells in Fig. 9. The number of molecules participate in forming this structure only is larger than we estimated from the larger structure in Fig. 9. There are two reasons for this phenomenon. First, in the simulation of 192 molecules, the molecules are more scattered at the starting point so small fraction of them were not assembled to the "Y"-shape structure. Second, with this structure only in the solvent condition, more molecules participate in to cover the inner hydrophobic core from the water molecules.

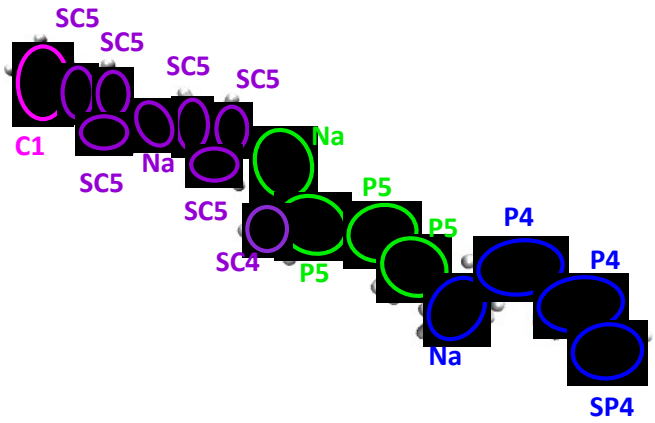

Fig. S9 The mapping scheme from atomistic structure to Martini beads.

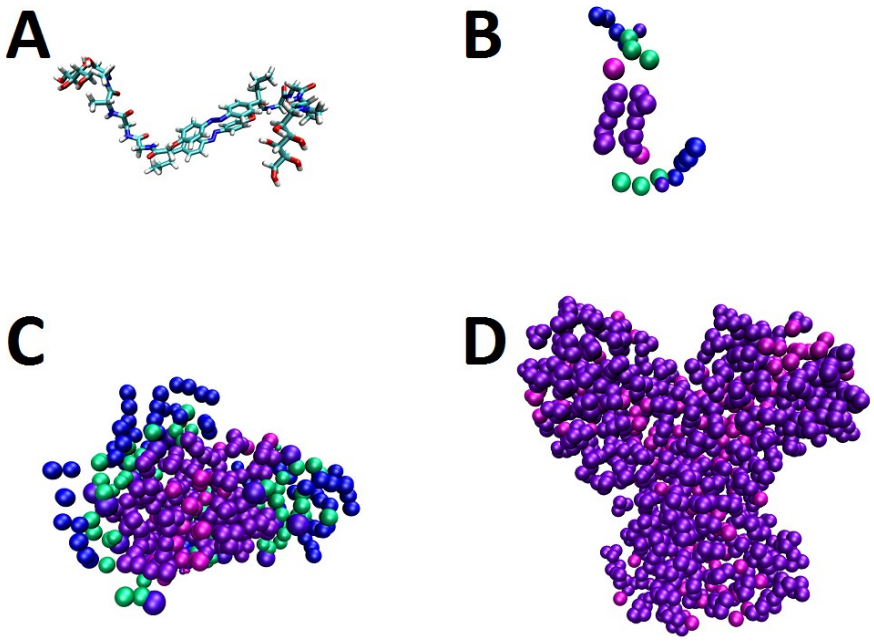

Fig. S10 Atomistic (A) and coarse-grained (B) bi-molecule structure of AGP3 and representative simulation results of AGP1 with different number of molecules in solvated systems: (C) 32 molecules and (D) 192 molecules (inner hydrophobic scaffold only for structural clarity). All solvent molecules both atomistic simulations and coarse-grained simulations were taken off for Figure clarity.

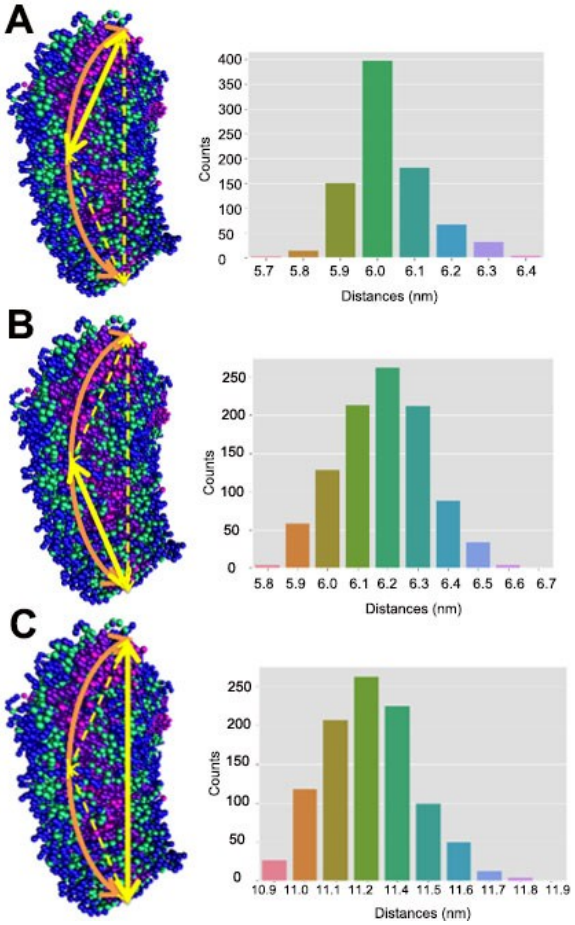

Fig. S11 Histogram plots of characteristic distances (as indicated by the solid yellow arrowed lines) of AGP1 assembly between atom (A) 508-C1 and 77-C1; (B) 77-C1 and 736-C1; (C) 736-C1 and 508-C1. The corresponding curvature is calculated to be 0.13 nm^{-1}.

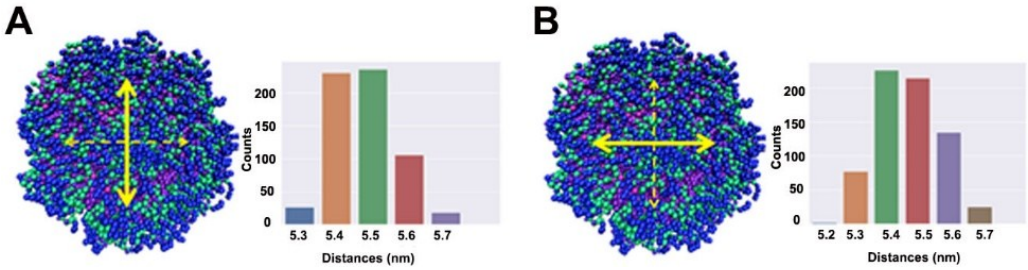

Fig. S12 Histogram plots of characteristic distances (as indicated by the solid yellow arrowed lines) of GGA assembly between atom (A) 508-C1 and 77-C1; (B) 77-C1 and 736-C1. The corresponding curvature is calculated to be 0.37 nm-1.

3) Simulation details for atomistic simulations

For both straightforward atomistic and Metadynamics MD simulations, a time step of 2 fs was used for 1ns in a cubic simulation box with the side of 6 nm. The simulation boxes with periodic boundary conditions were filled with 6,956 SPC-type water molecules. For the Metadynamics MD simulation, the distances between two (-N=N-) groups from separated molecules were selected as the collective variable. The distance ranges from 0.1 to 6 nm as the size of the box with a grid size of 0.1 nm. All simulations in this work were performed with a canonical ensemble (NVT) at 300 K.

4) Simulation details for Martini coarse-grained simulations

Martini-type coarse-grained models were used. The general guideline of Martini models is to use each coarse-grained bead to represent 2 to 4 heavy atoms in a group from the atomistic structures. Accordingly, several parameterization methods were developed under this guideline for different type of molecules.[8] The resulting mapping from atomistic structures and the Martini beads were labeled in the Fig. S9.

The details of Martini coarse-grained simulations of different system sizes were listed in Table S1. All simulations were performed at 300 K. Standard Martini water particles were used, each of which represents 4 water molecules of all-atom structures.

Table S1. Simulation details for Martini coarse-grained simulations.

Number of molecules	Number of water particles	Box size (nm)	Equilibrium time (ns) / Step size (fs)	Production time (ns) / Step size (fs)
2	1,620	5.8	0.2/ 1	5/ 5
8	1,559	5.8	0.2/ 1	5/ 5
32	3,632	7.7	0.2/ 1	200/ 5
128	16,081	12.7	0.4/ 1	400/ 10
192	25,728	14.8	0.4/ 1	800/ 20
784	50,602	26.4/ 9.81	0.6/ 1	950/ 20

[1]The largest simulation system was performed in a box (26.4*26.4*9.8), while all other simulations were performed in cubic boxes. As discussed, the molecule positions in this large system were initialized into spaced two-layer formation.

Antibiofilm activity of AGP assemblies

1) Biofilm inhibition assays

The amount of biofilm formation in 96-well plates was determined by a microtiter dish method which allows for the formation of a biofilm on the wall and/or bottom of a microtiter dish.[10] 100 μL of bacterial suspension (2×10^4 cells mL^{-1} of *S. aureus* in 2×TSB) was incubated with 100 μL of PBS solution containing 1.2 mM of AGP1, AGP2, AGP3, AGP1/β-CyD or AGP1/β-CyD/ADA at 37 °C in dark for 24 h to allow biofilm formation (each sample was tested in five wells), following which the plates were gently washed 3 times with water to remove unattached bacterial cells and media components. ① The plates were then kept at 55 °C for 1 h to rigidly fix the biofilms to the plates, followed by staining the biofilms with 200 μL of crystal violet (0.1% w/v in water) at 37 °C for 15 min. The plates were then exposed to running water until free crystal violet stops releasing from the biofilms. The biofilms were then dried overnight in air, followed by addition of 200 μL of acetic acid (30% v/v in water) to each well to solubilize the crystal violet taken up by the bacterial biofilms. The solubilized crystal violet was monitored at OD_{550} using a Thermo Scientific Varioskan LUX Multimode Microplate Reader. ② The formed biofilm in 96-well plates was stained with LIVE/DEAD™ BacLight™ Bacterial Viability Kit and visualized by ZEISS Axio Vert.A1 fluorescent microscopy imaging system.

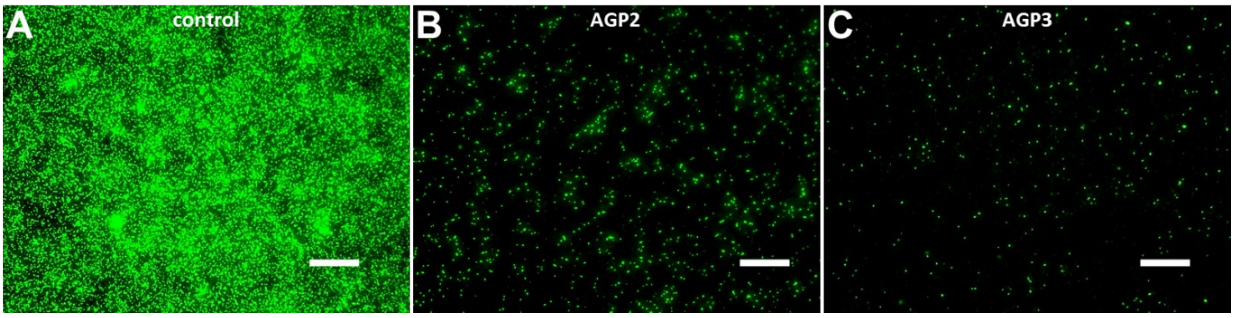

Fig. S13 Fluorescent microscopy imaging of the formed *S. aureus* biofilms in the presence of PBS (B, as a control), 0.6 mM of AGP2 or AGP3 for 24 h at 37 °C after SYTO9-staining. The scale bars are 20 μm.

2) Biofilm elimination assays

200 μL of bacterial suspension (10^6 cells mL^{-1} of *S. aureus* in TSB) was seeded in 96-well plates and incubated at 37 °C in dark for 24 h. After biofilm formation, the preformed *S. aureus* biofilm was incubated with 200 μL of PBS solution containing 0.6 mM of AGP1, AGP2, AGP3, AGP1/β-CyD, or AGP1/β-CyD/ADA at 37 °C in dark for 24 h. ① Afterward, the medium was aspirated, following which the metabolic activity of the treated biofilm was quantified by the 2,3-bis(2-methoxy-4-nitro-5-sulfophenyl)-2H-tetrazolium-5-arboxanilide (XTT) reduction assay, which characterizes living biomass. Briefly, XTT was freshly dissolved in PBS at a final concentration of 1 mg mL^{-1}. Menadione alcohol solution (0.4 mM) was also prepared. Before each assay, XTT solution was mixed with menadione solution at a volume ratio of 20 : 1. The XTT-menadione solution (200 μL) was then added to each well. The microtiter plates were then incubated in the dark for 1 h at 37 °C. Following incubation, the color change resulting from XTT reduction was measured at 490 nm with a Thermo Scientific Varioskan LUX Multimode Microplate Reader. ② Afterward, the medium was aspirated, following which the amount of the treated biofilms was quantified by the crystal violet assay that does not differentiate between live and dead bacterial cells. ③ For biofilm morphological study, the treated biofilm was stained with LIVE/DEAD™ BacLight™ Bacterial Viability Kit and observed by a ZEISS Axio Vert.A1 fluorescent microscopy imaging system.

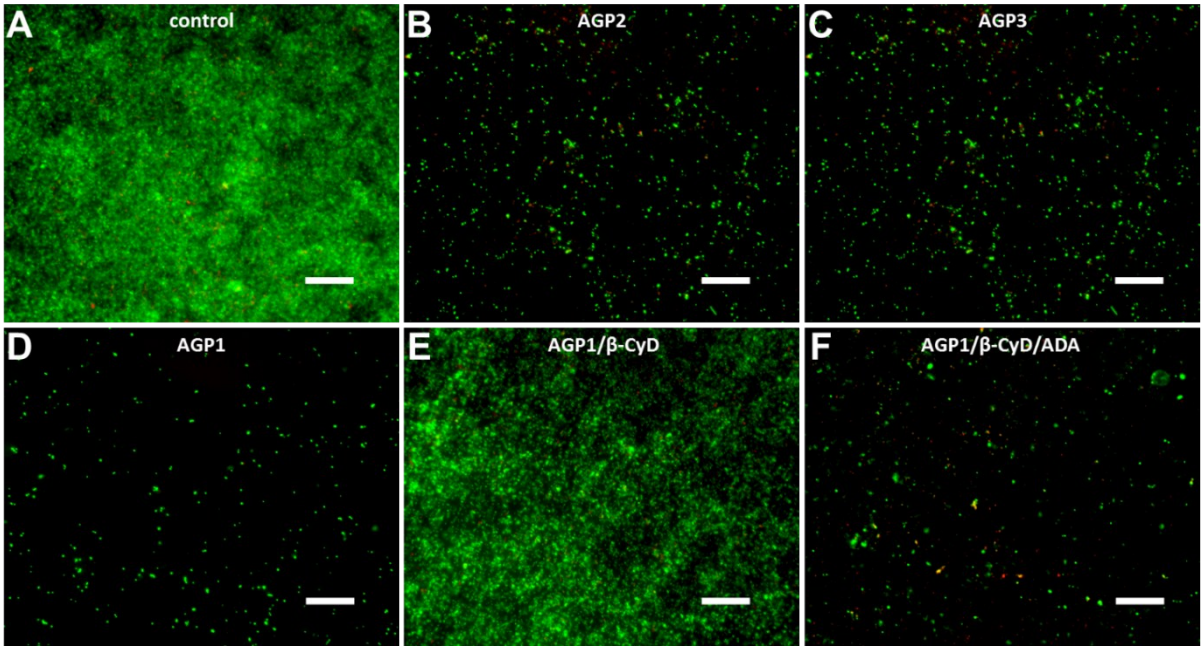

Fig. S14 Fluorescent microscopy imaging of the preformed *S. aureus* biofilms after treatment of PBS (A, as a control), 0.6 mM of AGP1, AGP2, AGP3, AGP1/β-CyD or AGP1/β-CyD/ADA for 24 h at 37 ^{o}C after staining with LIVE/DEAD^{TM} BacLight^{TM} Bacterial Viability Kit (live cells appear green, dead cells appear red; scale bar = 20 μm).

References

[1] a) Y. Lin, A. Wang, Y. Qiao, C. Gao, M. Drechsler, J. Ye, Y. Yan, J. Huang, *Soft Matter* **2010**, *6*, 2031. b) X. Song, J. Perlstein, D. Whitten, *J. Am. Chem. Soc.* **1997**, *119*, 9144-9159.

[2] M. D. Hanwell, D. E. Curtis, D. C. Lonie, T. Vandermeersch, E. Zurek, G. R. Hutchison, *J. Cheminform.* **2012**, *4*, 17.

[3] W. Humphrey, A. Dalke, K. Schulten, *J. Molec. Graphics* **1996**, *14*, 33-38.

[4] a) H. J. C. Berendsen, D. van der Spoel, R. van Drunen, *Comp. Phys. Comm.* **1995**, *91*, 43-56; b) E. Lindahl, B. Hess, D. van der Spoel, *J. Mol. Model* **2001**, *7*, 306-317; c) D. van der Spoel, E. Lindahl, B. Hess, G. Groenhof, A. E. Mark, H. J. Berendsen, *J. Comput. Chem.* **2005**, *26*, 1701-1718; d) B. Hess, C. Kutzner, D. van der Spoel, E. Lindahl, *J. Chem. Theory Comput.* **2008**, *4*, 435-447; e) S. Pronk, S. Páll, R. Schulz, P. Larsson, P. Bjelkmar, R. Apostolov, M. R. Shirts, J. C. Smith, P. M. Kasson, D. van der Spoel, B. Hess, E. Lindahl, *Bioinformatics* **2013**, *29*, 845-854; f) P. Szilárd, M. J. Abraham, C. Kutzner, B. Hess, E. Lindahl, *Proc. EASC* **2014**, *8759*, 3-27; g) M. J. Abraham, T. Murtola, R. Schulz, S. Páll, J. C. Smith, B. Hess, E. Lindahl, *SoftwareX* **2015**, *1-2*, 19-25.

[5] A. Laio, M. Parrinello, *Proc. Natl. Acad. Sci. U.S.A.* **2002**, *99*, 12562-12566.

[6] G. A. Tribello, M. Bonomi, D. Branduardi, C. Camilloni, G. Bussi, *Comp. Phys. Comm.* **2014**, *185*, 604-613.

[7] J. A. Graham, J. W. Essex, S. Khalid, *J. Chem. Inf. Model.* **2017**, *57*, 650-656.

[8] a) S. J. Marrink, D. P. Tieleman, *Chem. Soc. Rev.* **2013**, *42*, 6801-6822; b) D. H. de Jong, G. Singh, W. F. D. Bennett, C. Arnarez, T. A. Wassenaar, L. V. Schäfer, X. Periole, D. P. Tieleman, S. J. Marrink, *J. Chem. Th. Comp.* **2013**, *9*, 687-697; c) X. Periole, S. J. Marrink, L. Monticelli, E. Eds. Salonen, Springer, Vol 924, **2013**, pp 533-565. d) S. O. Yesylevskyy, L. V. Schäfer, D. Sengupta, S. J. Marrink, *PLoS Comp. Biol.* **2010**, *6*, e1000810; e) C. A. Lopez, A. Rzepiela, A. H. de Vries, L. Dijkhuizen, P. H. Huenenberger, S. J. Marrink, *J. Chem. Th. Comp.* **2009**, *5*, 3195-3210; f) S. J. Marrink, M. Fuhrmans, H. J. Risselada, X. Periole, G. ed. Voth, CRC press, Chapter 2, **2008**; g) L. Monticelli, S. K. Kandasamy, X. Periole, R. G. Larson, D. P. Tieleman, S. J. Marrink, *J. Chem. Th. Comp.* **2008**, *4*, 819-834.

[9] a) S. J. Marrink, A. H. de Vries, A. E. Mark, *J. Phys. Chem. B* **2004**, *108*, 750-760; b) S. J. Marrink, H. J. Risselada, S. Yefimov, D. P. Tieleman, A. H. de Vries, *J. Phys. Chem. B* **2007**, *111*, 7812-7824.

[10] G. A. O'Toole, *J. Vis. Exp.* **2011**, *47*, 2347.